

Widespread woody plant use of water stored in bedrock

<https://doi.org/10.1038/s41586-021-03761-3>

Received: 30 December 2020

Accepted: 22 June 2021

Published online: 8 September 2021

 Check for updates

Erica L. McCormick¹✉, David N. Dralle², W. Jesse Hahm³, Alison K. Tune¹, Logan M. Schmidt¹, K. Dana Chadwick¹ & Daniella M. Rempe¹

In the past several decades, field studies have shown that woody plants can access substantial volumes of water from the pores and fractures of bedrock^{1–3}. If, like soil moisture, bedrock water storage serves as an important source of plant-available water, then conceptual paradigms regarding water and carbon cycling may need to be revised to incorporate bedrock properties and processes^{4–6}. Here we present a lower-bound estimate of the contribution of bedrock water storage to transpiration across the continental United States using distributed, publicly available datasets. Temporal and spatial patterns of bedrock water use across the continental United States indicate that woody plants extensively access bedrock water for transpiration. Plants across diverse climates and biomes access bedrock water routinely and not just during extreme drought conditions. On an annual basis in California, the volumes of bedrock water transpiration exceed the volumes of water stored in human-made reservoirs, and woody vegetation that accesses bedrock water accounts for over 50% of the aboveground carbon stocks in the state. Our findings indicate that plants commonly access rock moisture, as opposed to groundwater, from bedrock and that, like soil moisture, rock moisture is a critical component of terrestrial water and carbon cycling.

Plant transpiration mediates water and energy exchange at Earth's surface. The circulation of near-surface water by plant roots has consequences for a large number of Earth-system processes, including landscape evolution, ecosystem carbon storage and nutrient delivery to streams⁶. At present, soils (physically mobile regolith) are thought to store the majority of root-zone water. As a result, soil processes underpin the conceptual frameworks and models used to predict environmental change. For example, climate projections rely on large-scale estimates of soil hydraulic properties⁷.

However, plants can source water and nutrients from bedrock⁸, which is exposed or only thinly soil-mantled across much of Earth's terrestrial surface⁹. Unlike soils, bedrock is characterized by relict primary rock structures, such as bedding or joint planes, which manifest distinct hydraulic¹⁰ and biological¹¹ processes.

Recent field studies have indicated that plants can access substantial volumes of rock moisture^{1,4}, defined as plant-available water stored in unsaturated, weathered bedrock³. Furthermore, the water storage capacity of bedrock can explain ecosystem distributions and drought vulnerability^{12–14}. In the face of widespread drought-induced die off^{15,16}, massive wildfires¹⁷ and woody encroachment¹⁸, information about the spatial and temporal patterns of plant-available water in bedrock is needed to appropriately predict water and carbon fluxes under environmental change.

Here we quantify root-zone water storage in bedrock across the continental United States (CONUS) using publicly available data. We estimate lower bounds on the magnitude and frequency of bedrock water use by plants, and map the spatial distribution of plant access to bedrock water.

Results and discussion

Bedrock water sustains transpiration

Over 45% of the wooded land area across the CONUS is underlain by shallow (<1.5 m deep) bedrock (Fig. 1). These areas are distributed across a broad range of environments (Fig. 2), consistent with previous mapping of the distribution of weathered bedrock across the CONUS⁹. A compilation of field studies reporting rooting into bedrock (locations shown as points in Fig. 2b) confirms that roots penetrate bedrock across a broad range of plant species, climates and rock types globally (Methods).

To quantify where bedrock water is routinely accessed by woody vegetation, we calculated a lower bound on the volume of bedrock water accessed by plants in a given water year ($D_{\text{bedrock},Y}$, bedrock water storage deficit in water year Y) for areas where woody vegetation overlies shallow bedrock. The spatial distribution of $D_{\text{bedrock},Y}$ is mapped in Figs. 2, 3 (Methods, Extended Data Fig. 1). In locations shown in black in Fig. 2, $D_{\text{bedrock},Y}$ is zero in all years, meaning that soil water storage capacity is sufficient to explain the observed evapotranspiration (ET). However, in many areas across the CONUS, soil water storage capacity is insufficient to explain ET (that is, $D_{\text{bedrock},Y}$ is commonly greater than zero; pink and green in Fig. 2), and, therefore, bedrock must supply water for transpiration. Green areas, where $D_{\text{bedrock},Y}$ is greater than zero across all study years, indicate routine use of bedrock water for transpiration. These locations host substantial aboveground biomass. For example, woody vegetation that withdraws bedrock water for ET on an annual basis (green in Fig. 2) accounts for over 50% of California's aboveground carbon stocks¹⁹ (587 Tg of carbon) (Extended Data Fig. 2a).

¹Department of Geological Sciences, Jackson School of Geosciences, University of Texas at Austin, Austin, TX, USA. ²Pacific Southwest Research Station, United States Forest Service, Davis, CA, USA. ³Department of Geography, Simon Fraser University, Burnaby, British Columbia, Canada. ✉e-mail: erica.mccormick@utexas.edu

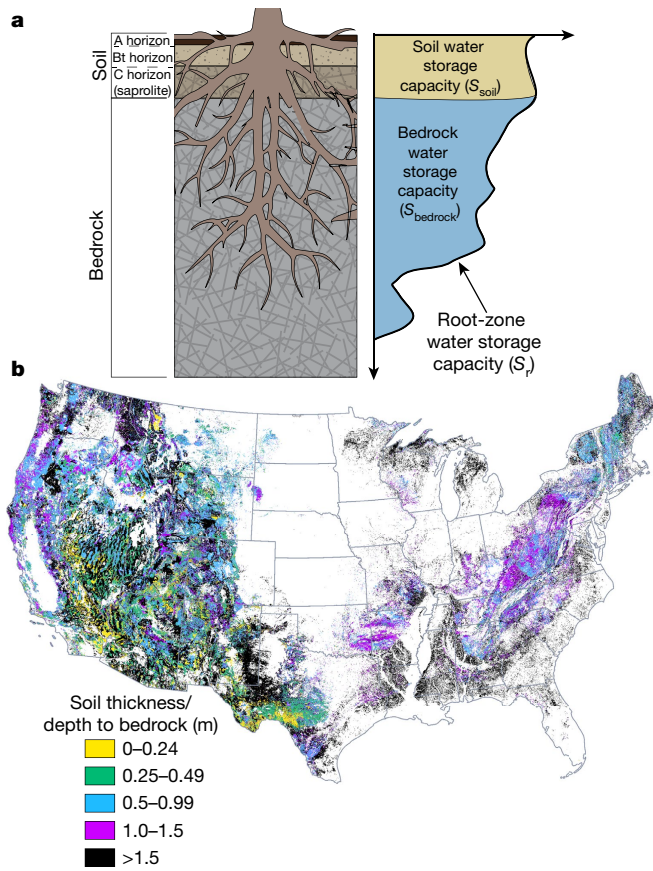


Fig. 1 | Over 45% of the wooded land area across the CONUS is underlain by shallow (<1.5 m deep) bedrock. **a**, Conceptual diagram of a root-zone including bedrock (left) and a depth profile of root-zone water storage capacity (right). The root-zone water storage capacity is partitioned into soil and bedrock components. **b**, The extent of woody vegetation is coloured by soil thickness, which could also be considered the depth to bedrock because only areas mapped as underlain by bedrock are shown. Landcover data were sourced from the USGS NLCD⁴⁰ and soil thickness from the USDA gNATSGO⁴¹. All raster maps in all figures and Extended data were plotted in QGIS⁴², with map data generated in Python in the Google Colaboratory environment. All raster data are publicly available and were processed using the Google Earth Engine Python application programming interface (API).

The magnitude and spatial distribution of $D_{\text{bedrock},Y}$ across California and Texas are reported in Fig. 3a. In any given year, transpiration is at least partially sourced from bedrock over at least 28–30% and 5–10% of the total land areas of California and Texas, respectively (Fig. 3a). $D_{\text{bedrock},Y}$ for all of the CONUS is reported in Extended Data Fig. 3. In some areas, $D_{\text{bedrock},Y}$ exceeds 300 mm and can constitute more than one-quarter of the mean annual precipitation (Extended Data Fig. 4). Bedrock is thus a critical storage reservoir of plant-accessible water over large areas. We focus here on California and Texas because bedrock water use has been documented via field studies in those states (Fig. 3b) and they experience extended dry periods where deficits reflecting storage volumes can accumulate.

Deficit-based methods, such as those employed here, yield lower-bound estimates of root-zone water storage (Methods); however, where there are long, extended dry periods or where energy and precipitation delivery are out of phase, deficit-based estimates of root-zone storage are more likely to approach actual root-zone storage capacity. By contrast, where precipitation occurs year-round or where energy and precipitation delivery are in phase, deficit-based methods will more substantially underestimate root-zone storage capacity. This is because withdrawal from storage (that is, ET) during extended

dry periods will cause increases in an accrued deficit, whereas ET during periods with frequent precipitation will not result in a large accrued deficit.

We calculate a bedrock root-zone water storage capacity, S_{bedrock} , which is defined as the largest storage used by woody vegetation over a multiyear time window (2003–2017) that cannot be accounted for by soil water storage capacity (Methods, Extended Data Fig. 5). S_{bedrock} as a percentage of total root-zone storage capacity is reported in Fig. 4, which shows that bedrock water storage often constitutes the majority of total storage capacity in the root zone.

In some locations, the magnitude of $D_{\text{bedrock},Y}$ is relatively consistent across different years, and consequently similar to S_{bedrock} , indicating that plants withdraw similar amounts of bedrock water each year. However, in other locations, such as the southern Sierra Nevada in California and the Edwards Plateau in Texas, S_{bedrock} is often larger than $D_{\text{bedrock},Y}$ (Extended Data Figs. 3, 5), indicating that the storage capacity of plant-accessible water in bedrock is much greater than the storage that is withdrawn in a given year. Under these conditions, bedrock may have a central role in plant response to multiyear drought because bedrock water is progressively drawn down to explain the observed ET²⁰.

Bedrock water serves as a reservoir for transpiration in locations hosting high aboveground biomass (Extended Data Fig. 2a) across a range of biomes and Köppen climate types, including humid climates (Extended Data Fig. 6). The largest measurements of S_{bedrock} are associated with arid, semiarid and Mediterranean climate types and evergreen forests, savannahs and shrublands (Extended Data Fig. 6, Extended Data Table 1). Bedrock water storage may be particularly important in semiarid shrublands, Mediterranean savannahs and Mediterranean needleleaf forests (Extended Data Table 1).

Rock moisture commonly accessed

Locations where field studies document plant use of unsaturated bedrock water storage (that is, rock moisture) coincide with locations where we calculate positive median $D_{\text{bedrock},Y}$ (Fig. 3b, Extended Data Fig. 7). This corroborates our use of $D_{\text{bedrock},Y}$ as an indicator of ecosystem access to bedrock water stores. Field studies reporting greater than 50% of annual ET derived from rock moisture are shown in Fig. 3b. Some of these sites do not meet our analysis criteria (Methods) and are consequently masked (designated with superscripts in Fig. 3b, Extended Data Fig. 7). This is another indication that our reported values are underestimates of the spatial extent of bedrock water use, and thus the volume of bedrock water accessed (Methods). Although bedrock water storage volumes measured at these sites are calculated using very different methods from those employed here, there is general agreement between $D_{\text{bedrock},Y}$ (shown as blue bars in Fig. 3b) and field measurements of bedrock water storage accessed by plants (shown as circles in Fig. 3b).

Bedrock water storage used by plants can commonly occur in the form of rock moisture (Fig. 3b, Extended Data Fig. 7); however, $D_{\text{bedrock},Y}$ and S_{bedrock} do not discriminate between rock moisture (unsaturated) and bedrock groundwater (saturated). Even in field settings, partitioning plant water use between the unsaturated and saturated zones remains challenging, yet the distinction between them is germane to mechanistically modelling biogeochemical and hydraulic processes. Rock moisture use has been confirmed under circumstances that might commonly be attributed to groundwater use. For example, Hahm et al.²¹ have shown that oaks relied on rock moisture to sustain dry season transpiration at an oak savannah site where groundwater remains within 3 m of the surface throughout the year. Insensitivity of ET to extended drought is another tool used to attribute groundwater as a transpiration source; however, storage capacity in the unsaturated zone can produce similar insensitivity of ET to drought¹². These circumstances suggest that misattribution of rock moisture as groundwater is likely, and that rock moisture use by woody plants may be common.

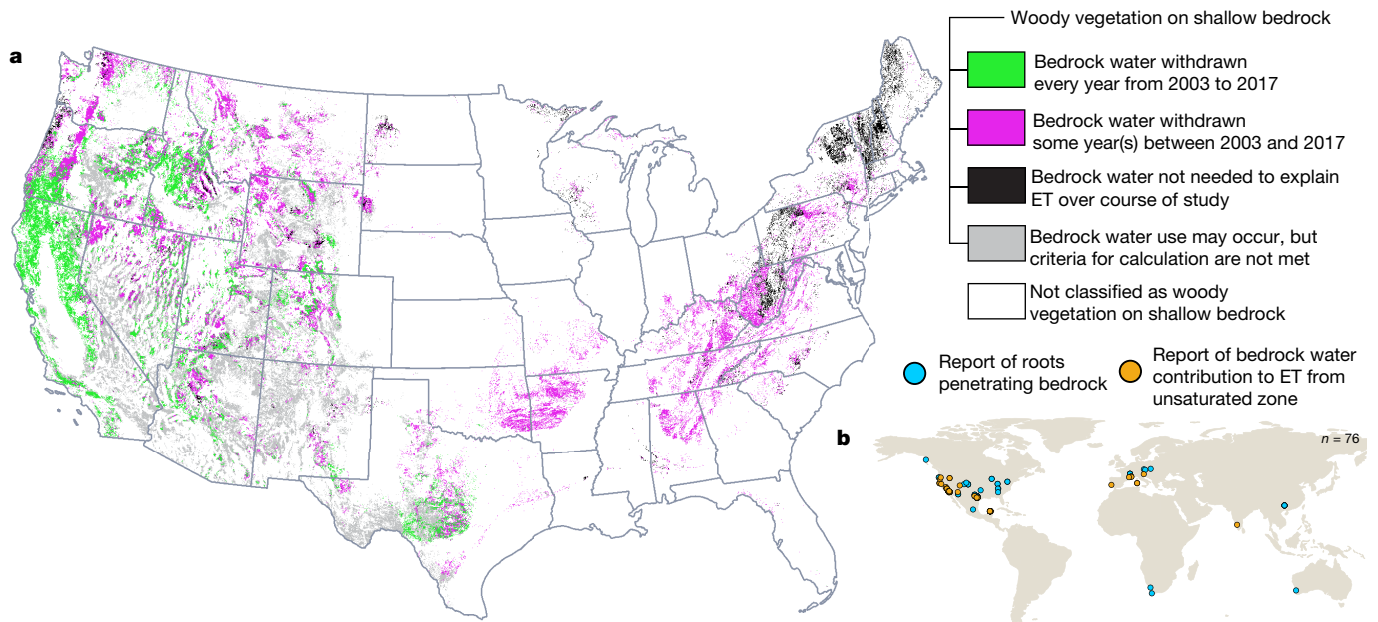


Fig. 2 | Bedrock water use by woody plants is spatially extensive and can be routine. **a**, The occurrence of bedrock water withdrawal by woody plants in the CONUS from 2003 to 2017. Coloured areas indicate the extent of woody vegetation where bedrock is encountered within the upper 1.5 m. This area is divided into four colours reflecting locations where the annual bedrock water storage deficit ($D_{\text{bedrock},y}$) is greater than zero for every year of the study (green), $D_{\text{bedrock},y}$ is greater than zero for at least one year of the study (pink), $D_{\text{bedrock},y}$ is not greater than zero for any years of the study (black) and $D_{\text{bedrock},y}$ is not reported because our analysis criteria are not met (grey; Methods). An annual

$D_{\text{bedrock},y}$ value of greater than zero in a given location indicates that the withdrawal of bedrock water is necessary to explain observed ET (Methods). Landcover data were sourced from the USGS NLCD⁴⁰ and depth to bedrock from the USDA gNATSGO⁴¹. **b**, Global map showing the locations of field studies where rooting into bedrock has been reported (blue) and where rock moisture (that is, bedrock water in the unsaturated zone) has been observed or measured as a contribution to ET (orange). The vector map was generated in Python with data from the literature review (Methods).

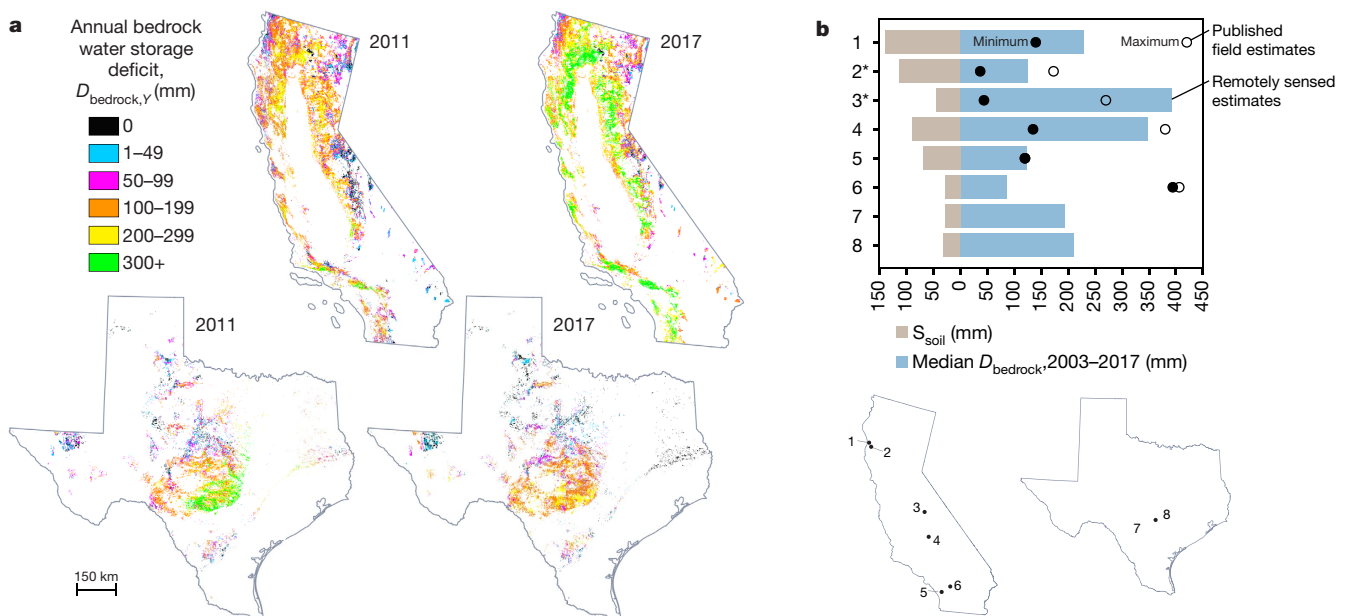


Fig. 3 | Magnitude of bedrock water contribution to ET across Texas, California and field studies. **a**, Magnitude of annual bedrock water storage deficit ($D_{\text{bedrock},y}$) across California (top) and Texas (bottom) for the years 2011 and 2017, which represent high variation in $D_{\text{bedrock},y}$. $D_{\text{bedrock},y}$ for all of the CONUS is shown in Extended Data Fig. 3. **b**, Soil water storage capacity (S_{soil} , brown) and median $D_{\text{bedrock},2003-2017}$ (blue) across sites where previous studies report that over 50% of ET is derived from rock moisture, that is, bedrock water

storage in the unsaturated zone. The volume of bedrock water use reported for each study is shown as closed circles (minimum estimates) or open circles (maximum estimates) where available. Site locations are shown at the bottom. Asterisks denote locations where soil depths are greater than 1.5 m (ref. ⁴¹), and thus are masked from maps reporting $D_{\text{bedrock},y}$ or $S_{\text{bedrock},y}$. References for field studies: 1, refs. ^{2,3}, 2, refs. ^{3,21}, 3, refs. ^{4,43}, 4, refs. ^{5,44,45}, 5, refs. ^{6,46}, 6, refs. ^{7,47,48}, 7, refs. ^{8,49}, 8, refs. ^{1,50}. Data in **b** are from the literature review (Methods).

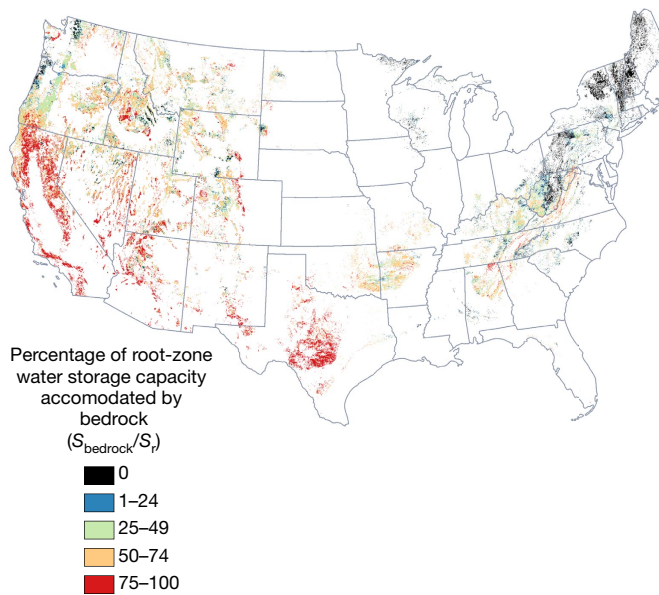


Fig. 4 | Bedrock hosts a large fraction of root-zone water storage capacity.

The percentage of root-zone water storage capacity that can be attributed to bedrock in areas that meet our analysis criteria (Methods). The magnitude of the bedrock water storage deficit (S_{bedrock}) is shown in Extended Data Fig. 5.

Implications of bedrock water uptake

Although it has long been recognized that woody plants root into bedrock²², the widespread and routine transpiration of bedrock water reported here suggests that the dynamics of bedrock water storage may be as fundamental to understanding terrestrial water and carbon cycling as soil moisture. Across the western United States in particular, large volumes of water are stored in bedrock and released back into the atmosphere on an annual basis. For example, our deficit analysis suggests that in California alone, 20 km³ (16.2 million acre-feet) of water can be extracted from bedrock by woody plants annually. This is approximately equal to the volume of water stored in all of the state's reservoirs combined²³, and about three times the state's annual domestic water use²⁴. Although our study is limited to the CONUS, bedrock water use by woody vegetation has also been documented in a wide range of environments globally^{25–32}.

Investigation of biological and hydraulic processes in the bedrock rhizosphere is a frontier research area^{4–6}. New studies are needed to clarify the role of bedrock water storage under projected shifts in global precipitation regimes, including multiyear drought and alternation between extreme wet and dry years. In the 2011–2016 California drought, for example, forest ecosystems with access to rock moisture exhibited diverse responses, from insensitivity¹² to vulnerability²⁰. This motivates new field-based observational studies of belowground structure and bedrock water storage dynamics across diverse lithological, climatic and ecological settings to clarify the different ways in which bedrock water storage mediates ecohydrological processes^{33,34}.

Plant bedrock water use, and specifically the use of rock moisture, occurs in critical locations for water supply, including the Sierra Nevada, the recharge zone of the Edwards and Trinity aquifers, and the headwaters of the Colorado River (Figs. 2, 3), which together supply water to at least one-quarter of the US population. Given that the dynamics of rock moisture have the potential to regulate the timing of groundwater recharge and runoff³⁵, bedrock water storage may be critical to water resource planning.

Woody ecosystem dependence on stored subsurface water will probably increase in the future as plant community ranges shift³⁶, snowpack declines in high-elevation and high-latitude regions, and

many environments undergo a transition from energy-limited to water-limited conditions³⁷. Thus, the availability of bedrock water storage may be key to predicting large-scale vegetation dynamics, including the stability or vulnerability of ecosystem carbon storage, under climate change.

Long-term, intensive monitoring studies are increasingly documenting mechanisms by which roots in bedrock impact ecosystem function¹³, groundwater and stream chemistry³⁸, and rates of soil production and weathering⁶. Although bedrock water storage in the humid eastern USA may be largely undetectable via a deficit-based water balance, substantial circulation of water in bedrock may be occurring. This could lead to largely unmeasured drivers of carbon cycling³⁹. Thus, bedrock water storage dynamics are likely key to understanding the sensitivity of carbon, water and latent heat fluxes to changes in climate.

Online content

Any methods, additional references, Nature Research reporting summaries, source data, extended data, supplementary information, acknowledgements, peer review information; details of author contributions and competing interests; and statements of data and code availability are available at <https://doi.org/10.1038/s41586-021-03761-3>.

1. Schwinnning, S. The ecohydrology of roots in rocks. *Ecohydrology* **3**, 238–245 (2010).
2. Rose, K., Graham, R. & Parker, D. Water source utilization by *Pinus jeffreyi* and *Arctostaphylos patula* on thin soils over bedrock. *Oecologia* **134**, 46–54 (2003).
3. Rempe, D. M. & Dietrich, W. E. Direct observations of rock moisture, a hidden component of the hydrologic cycle. *Proc. Natl Acad. Sci. USA* **115**, 2664–2669 (2018).
4. Schwinnning, S. A critical question for the critical zone: how do plants use rock water? *Plant Soil* **454**, 49–56 (2020).
5. Fan, Y. et al. Hillslope hydrology in global change research and Earth system modeling. *Wat. Resour. Res.* **55**, 1737–1772 (2019).
6. Brantley, S. L. et al. Reviews and syntheses: on the roles trees play in building and plumbing the critical zone. *Biogeosciences* **14**, 5115–5142 (2017).
7. Chaney, N. W. et al. POLARIS soil properties: 30-m probabilistic maps of soil properties over the contiguous United States. *Wat. Resour. Res.* **55**, 2916–2938 (2019).
8. Uhlig, D., Schuessler, J. A., Bouchez, J., Dixon, J. L. & Blanckenburg, F. V. Quantifying nutrient uptake as driver of rock weathering in forest ecosystems by magnesium stable isotopes. *Biogeosciences* **14**, 3111–3128 (2017).
9. Wald, J. A., Graham, R. C. & Schoeneberger, P. J. Distribution and properties of soft weathered bedrock at 1 m depth in the contiguous United States. *Earth Surf. Process. Landf.* **38**, 614–626 (2013).
10. Nimmo, J. R., Creasey, K. M., Perkins, K. S. & Mirus, B. B. Preferential flow, diffuse flow, and perching in an interbedded fractured-rock unsaturated zone. *Hydrogeol. J.* **25**, 421–444 (2017).
11. Leshem, B. Resting roots of *Pinus halepensis*: structure, function, and reaction to water stress. *Bot. Gaz.* **131**, 99–104 (1970).
12. Hahm, W. J. et al. Low subsurface water storage capacity relative to annual rainfall decouples Mediterranean plant productivity and water use from rainfall variability. *Geophys. Res. Lett.* **46**, 6544–6553 (2019).
13. Hahm, W. J. et al. Lithologically controlled subsurface critical zone thickness and water storage capacity determine regional plant community composition. *Wat. Resour. Res.* **55**, 3028–3035 (2019).
14. Eggemeyer, K. D. & Schwinnning, S. Biogeography of woody encroachment: why is mesquite excluded from shallow soils? *Ecohydrology* **2**, 81–87 (2009).
15. Madakumbura, G. D. et al. Recent California tree mortality portends future increase in drought-driven forest die-off. *Environ. Res. Lett.* **15**, 124040 (2020).
16. McDowell, N. G. et al. Mechanisms of a coniferous woodland persistence under drought and heat. *Environ. Res. Lett.* **14**, 045014 (2019).
17. McEvoy, D. J., Pierce, D. W., Kalansky, J. F., Cayen, D. R. & Abatzoglou, J. T. Projected changes in reference evapotranspiration in California and Nevada: implications for drought and wildland fire danger. *Earth's Future* **8**, e2020EF001736 (2020).
18. Hauwert, N. M. & Sharp, J. M. Measuring autogenic recharge over a karst aquifer utilizing eddy covariance evapotranspiration. *J. Water Resour. Prot.* **6**, 869–879 (2014).
19. Spawn, S. A., Sullivan, C. C., Lark, T. J. & Gibbs, H. K. Harmonized global maps of above and belowground biomass carbon density in the year 2010. *Sci. Data* **7**, 112 (2020).
20. Goulden, M. L. & Bales, R. C. California forest die-off linked to multi-year deep soil drying in 2012–2015 drought. *Nat. Geosci.* **12**, 632–637 (2019).
21. Hahm, W. J. et al. Oak transpiration drawn from the weathered bedrock vadose zone in the summer dry season. *Wat. Resour. Res.* **56**, e2020WR027419 (2020).
22. Cannon, W. A. *The Root Habits of Desert Plants* 131 (Carnegie Institute of Washington, 1911).
23. Daily reservoir storage summary. California Department of Water Resources <https://info.water.ca.gov/cgi-progs/reservoirs/RES> (2020).
24. USGS water use data for California. United States Geological Society https://waterdata.usgs.gov/ca/nwis/water_use/ (2020).
25. David, T., Ferreira, M., Cohen, S., Pereira, J. & David, J. Constraints on transpiration from an evergreen oak tree in southern Portugal. *Agric. For. Meteorol.* **122**, 193–205 (2004).

26. Querejeta, J. I., Estrada-Medina, H., Allen, M. F. & Jimenez-Osornio, J. J. Water source partitioning among trees growing on shallow karst soils in a seasonally dry tropical climate. *Oecologia* **152**, 26–36 (2007).
27. Carrière, S. D. et al. The role of deep vadose zone water in tree transpiration during drought periods in karst settings—insights from isotopic tracing and leaf water potential. *Sci. Total Environ.* **699**, 134332 (2020).
28. Rambal, S. Water balance and pattern of root water uptake by a *Quercus coccifera* L. evergreen scrub. *Oecologia* **62**, 18–25 (1984).
29. Montaldo, N. et al. Rock water as a key resource for patchy ecosystems on shallow soils: digging deep tree clumps subsidize surrounding surficial grass. *Earth's Future* **9**, e2020EF001870 (2021).
30. Corona, R. & Montaldo, N. On the transpiration of wild olives under water-limited conditions in a heterogeneous ecosystem with shallow soil over fractured rock. *J. Hydrol. Hydromech.* **68**, 338–350 (2020).
31. Nardini, A. et al. Water ‘on the rocks’: a summer drink for thirsty trees? *New Phytol.* **229**, 199–212 (2021).
32. Ruiz, L. et al. Water balance modelling in a tropical watershed under deciduous forest (Mule Hole, India): regolith matrix storage buffers the groundwater recharge process. *J. Hydrol.* **380**, 460–472 (2010).
33. Ding, Y., Nie, Y., Chen, H., Wang, K. & Querejeta, J. I. Water uptake depth is coordinated with leaf water potential, water-use efficiency and drought vulnerability in karst vegetation. *New Phytol.* **229**, 1339–1353 (2021).
34. Dawson, T. E., Hahm, W. J. & Crutchfield-Peters, K. Digging deeper: what the critical zone perspective adds to the study of plant ecophysiology. *New Phytol.* **226**, 666–671 (2020).
35. Salve, R., Rempe, D. M. & Dietrich, W. E. Rain, rock moisture dynamics, and the rapid response of perched groundwater in weathered, fractured argillite underlying a steep hillslope. *Wat. Resour. Res.* **48**, W11528 (2012).
36. Harsch, M. A., Hulme, P. E., McGlone, M. S. & Duncan, R. P. Are treelines advancing? A global meta-analysis of treeline response to climate warming. *Ecol. Lett.* **12**, 1040–1049 (2009).
37. Kapnick, S. & Hall, A. Causes of recent changes in western North American snowpack. *Clim. Dyn.* **38**, 1885–1899 (2012).
38. Tune, A. K., Druhan, J. L., Wang, J., Bennett, P. C. & Rempe, D. M. Carbon dioxide production in bedrock beneath soils substantially contributes to forest carbon cycling. *J. Geophys. Res. Biogeosci.* **125**, e2020JG005795 (2020).
39. Hasenmueller, E. A. et al. Weathering of rock to regolith: the activity of deep roots in bedrock fractures. *Geoderma* **300**, 11–31 (2017).
40. Yang, L. et al. A new generation of the United States National Land Cover Database: requirements, research priorities, design, and implementation strategies. *ISPRS J. Photogramm. Remote Sens.* **146**, 108–123 (2018).
41. Soil Survey Staff *Gridded National Soil Survey Geographic (gNATSGO) Database for the Conterminous United States* (USDA, 2019); <https://nrcs.app.box.com/v/soils>
42. QGIS Development Team *QGIS Geographic Information System* (Open Source Geospatial Foundation, 2019); <http://qgis.org>
43. O’Geen, A. T. et al. Southern Sierra Critical Zone Observatory and Kings River Experimental Watersheds: a synthesis of measurements, new insights, and future directions. *Vadose Zone J.* **17**, 180081 (2018).
44. Anderson, M. A., Graham, R. C., Alyanakian, G. J. & Martynn, D. Z. Late summer water status of soils and weathered bedrock in a giant sequoia grove. *Soil Sci.* **160**, 415–422 (1995).
45. Hubbert, K. R., Graham, R. C. & Anderson, M. A. Soil and weathered bedrock: components of a Jeffrey pine plantation substrate. *Soil Sci. Soc. Am. J.* **65**, 1255–1262 (2001).
46. Bornyasz, M., Graham, R. & Allen, M. Ecotomycorrhizae in a soil-weathered granitic bedrock regolith: linking matrix resources to plants. *Geoderma* **126**, 141–160 (2005).
47. Sternberg, P., Anderson, M., Graham, R., Beyers, J. & Tice, K. Root distribution and seasonal water status in weathered granitic bedrock under chaparral. *Geoderma* **72**, 89–98 (1996).
48. Graham, R. C., Sternberg, P. D. & Tice, K. R. Morphology, porosity, and hydraulic conductivity of weathered granitic bedrock and overlying soils. *Soil Sci. Soc. Am. J.* **61**, 516–522 (1997).
49. McCole, A. A. & Stern, L. A. Seasonal water use patterns of *Juniperus ashei* on the Edwards Plateau, Texas, based on stable isotopes in water. *J. Hydrol.* **342**, 238–248 (2007).
50. Schwinning, S. The water relations of two evergreen tree species in a karst savanna. *Oecologia* **158**, 373–383 (2008).

Publisher’s note Springer Nature remains neutral with regard to jurisdictional claims in published maps and institutional affiliations.

© The Author(s), under exclusive licence to Springer Nature Limited 2021

Article

Methods

Literature compilation of rooting in bedrock

Available English-language published evidence of rooting into bedrock is included in our literature compilation⁵¹, which builds on several past compilations^{1,52–55}. Each entry includes information about rooting, climate, soil and bedrock properties. A subset of sites report use of rock moisture by vegetation. For these entries, where possible, we report estimates of the contribution of rock moisture to evapotranspiration, as well as any estimates of plant-available soil and rock moisture water storage capacities (Fig. 3b, Extended Data Fig. 7).

Landcover and soil datasets

To determine woody landcover, we used the evergreen, deciduous, mixed forest and shrub/scrub landcover classes reported by the United States Geological Survey (USGS) National Land Cover Database (NLCD)⁴⁰ at 30-m resolution. To determine areas underlain by bedrock within 1.5 m of the surface, and the available soil water storage capacity for those areas, we use the United States Department of Agriculture (USDA) Gridded National Soil Survey Geographic Database (gNATSGO) product at 90-m resolution⁴¹. gNATSGO data are generated using soil data from field surveys and subsequent laboratory analysis⁴¹. These surveys are occasionally repeated and the newest data are validated against historical surveys before replacement in the official nationwide database⁴¹.

To determine where bedrock underlies shallow soils, we use the gNATSGO product, which reports depths of soil restrictive layers for the classifications of lithic, densic and paralithic bedrock. Our calculation of bedrock water storage considers only areas where bedrock has been encountered within 1.5 m of the surface (Fig. 1, Extended Data Fig. 1). The 1.5 m depth is chosen because soil water storage capacity (S_{soil}) is only available across the CONUS to 1.5 m depth. Although bedrock water may be accessible to plants in areas with greater than 1.5 m soil depth, we exclude these areas because we cannot quantify S_{soil} there. We note that in practice, the interface between soil and bedrock has not been systematically mapped and the terminology used for defining that interface can be inconsistent⁹. The contact between soils and underlying bedrock can also be gradational and challenging to determine in the field. For example, saprolite, which can be defined as highly weathered bedrock that retains the original fabric of the rock, is often, but not always designated as a 'C' or 'Cr' horizon by the gNATSGO soil survey, and thus categorized as a soil in our study. Therefore, S_{soil} can include saprolite.

We estimate S_{soil} as the 'soil available water storage' (AWS) reported by the gNATSGO database⁴¹ (Extended Data Fig. 2b). This AWS product is calculated as the storage volume, in units of depth, between field capacity (~1/10 bar or ~1/3 bar) and wilting point (~15 bars) and is measured for each soil layer until contact with a bedrock restrictive layer. For each layer within a given soil profile, gNATSGO reports a high, low and likely value of AWS, which they take a thickness weighted average of to generate three estimates of profile total AWS. Here we use the highest reported value to represent the AWS of any given layer to avoid underestimating soil water storage. As the AWS product does not account for water stored between field capacity and saturation in soils, we tested the sensitivity of our results to the inclusion of this excess water by reporting S_{bedrock} and median $D_{\text{bedrock}, 2003–2017}$ for a hypothetical test case of double S_{soil} (Extended Data Fig. 8). We double S_{soil} to approximate the volume of water between field capacity and saturation. Doubling of S_{soil} necessarily reduces the magnitudes of S_{bedrock} ; however, the spatial area of positive S_{bedrock} is reduced by only 35%, indicating that underestimation of soil water storage capacity by a factor of two would still lead to a large volume of bedrock water use across the CONUS.

Masking procedure

We employ three masking criteria to constrain our analyses to places where (1) woody landcover occupies at least 75% of the 500-m pixel,

(2) all soils within the 500-m pixel are underlain by bedrock and less than 1.5 m deep, and (3) total evapotranspiration is less than total precipitation from 2003 to 2017 (Extended Data Fig. 1). The first two masking criteria restrict our calculations to places where water storage deficits could be explained by water extraction by woody plants from bedrock, because bedrock is near the surface and woody plants are present. The third masking criterion is employed to remove locations where outputs exceed inputs over long timespans, indicating either errors in fluxes or unmeasured fluxes entering the rooting zone, such as fog, dew, irrigation or lateral flow in soils. Bedrock water storage could be accessed in areas that do not meet these criteria, and indeed, there are several studies that report plant use of bedrock water in locations that are masked (Fig. 3b, Extended Data Fig. 7). However, in locations where our masking criteria fail to account for fog, dew or lateral inputs of water, bedrock water storage capacity may be overestimated (Methods).

Calculation of root-zone water storage capacity and maximum annual root-zone storage deficit

Here we use a statistically interpolated precipitation data product (Oregon State's PRISM daily precipitation^{56,57}) and a remotely sensed evapotranspiration product (Penman–Monteith–Leuning Evapotranspiration V2^{58,59}) to estimate the minimum magnitude of root-zone water storage capacity (S_r) following the method developed by Dralle et al.⁶⁰, which adapts the original method of S_r estimation from Wang–Erlandsson et al.⁶¹ to account for the presence of snow. All raster processing was conducted using the Google Earth Engine⁶² Python application programming interface (API).

The method takes a mass-balance approach and is therefore broadly applicable, not requiring place-based soil or plant-community parameterization⁶³. Specifically, the technique tracks a root-zone storage deficit (D) as a running, integrated difference between water fluxes exiting (F_{out}) in units of length per time [L/T] and entering (F_{in} [L/T]) the root zone, here taken to be evapotranspiration (ET) and precipitation (P), with $F_{\text{out}} = \text{ET}$ and $F_{\text{in}} = P$. This is accomplished by first computing the accumulated difference between F_{out} and F_{in} over a given time interval t_n to t_{n+1} :

$$A_{t_n \rightarrow t_{n+1}} = \begin{cases} 0 & \text{if } C \geq C_0 \\ \int_{t_n}^{t_{n+1}} (F_{\text{out}} - F_{\text{in}}) dt & \text{if } C < C_0 \end{cases}$$

where C_0 is the threshold percentage of areal snow cover deemed non-negligible, here chosen as 10%. This avoids attributing evapotranspiration from snowmelt recharge into the rooting zone to unreplenished water storage depletion. Snow data are acquired from the Normalized Difference Snow Index (NDSI) snow cover band from the 500-m MODIS/Terra data product⁶⁴.

With this, the root-zone storage deficit at any given time is defined iteratively as:

$$D(t_{n+1}) = \max(0, D(t_n) + A_{t_n \rightarrow t_{n+1}})$$

Following these equations, D at any given time represents a lower bound on the volume of water that plants have used that must have been withdrawn from root-zone storage without replenishment by precipitation. The deficit is effectively 'reset' to zero during wet periods, because the updated $D(t_{n+1})$ equals the maximum of 0 and the previous deficit plus the current difference between outgoing and incoming fluxes. Over the course of a year or many subsequent seasonal cycles, the maximum value of D represents the largest amount of subsurface water storage space that must have been used to supply ET.

Here we report two deficit-related quantities: the observed maximum root-zone storage deficit in water year Y ($D_{\text{max}, Y}$) and the maximum root-zone storage deficit over the period of record (2003–2017), taken as a lower bound on the actual root-zone storage capacity, S_r . $D_{\text{max}, Y}$ is

calculated for a given water year Y (that is, from 1 October in year $Y-1$ to 30 September in year Y) first by assuming the root-zone storage deficit on 1 October is zero, then tracking that deficit through to the end of the water year. $D_{\max,Y}$ is the maximum value of the deficit time series over that water year. The procedure for computing S_r is similar, but the deficit time series is computed over the period of record. That is, D is taken to be zero on 1 October 2003 and is tracked continuously until 30 September 2018. S_r is then taken to be the maximum value of this multiyear deficit time series. Importantly, S_r and D_{\max} are conservative lower estimates of water storage capacity and do not account for all possible withdrawal (see ‘Assumptions and limitations of deficit-based calculations of bedrock water storage’).

Bedrock root-zone water storage capacity and annual bedrock root-zone water storage

To quantify the root-zone storage capacity that cannot be accounted for by soil water storage capacity, S_{bedrock} , we subtract the soil water storage capacity from S_r , making sure to bound S_{bedrock} at zero:

$$S_{\text{bedrock}} = \begin{cases} 0 & \text{if } S_{\text{soil}} \geq S_r \\ S_r - S_{\text{soil}} & \text{if } S_{\text{soil}} < S_r \end{cases}$$

We perform a similar calculation to quantify the annual bedrock root-zone water storage capacity, $D_{\text{bedrock},Y}$, which is the maximum annual root-zone storage deficit that cannot be accounted for by soil water storage capacity:

$$D_{\text{bedrock},Y} = \begin{cases} 0 & \text{if } S_{\text{soil}} \geq D_{\max,Y} \\ D_{\max,Y} - S_{\text{soil}} & \text{if } S_{\text{soil}} < D_{\max,Y} \end{cases}$$

To attribute $D_{\text{bedrock},Y}$ and S_{bedrock} to transpiration of bedrock water by woody plants, we assume that evaporation is restricted to the soil layer, such that evaporation fluxes are accounted for by subtraction of S_{soil} from $D_{\max,Y}$ or S_r . Note that we use the highest AWS value reported. Therefore, S_{bedrock} and $D_{\text{bedrock},Y}$ are conservative lower bounds, as we use the upper bound on S_{soil} and the lower bound on S_r and $D_{\max,Y}$, respectively. The sensitivity of S_{bedrock} to S_{soil} is discussed above in ‘Landcover and soil datasets’.

Assumptions and limitations of deficit-based calculations of bedrock water storage

The methods we use to estimate the spatial pattern and magnitude of bedrock water use will provide a lower bound on bedrock water storage capacity, because (1) we employ a deficit-based water balance, (2) we use the largest available estimate of soil water storage capacity, and (3) we use masking criteria to exclude areas where alternative mechanisms might reasonably account for evapotranspiration. Here we explore the assumptions and limitations of our approach.

Deficit-based calculations of root-zone storage yield lower-bound estimates because they rely on fluxes to infer storage dynamics. That is, deficit-based methods cannot ‘detect’ the presence of a storage element if that storage does not supply a flux over the period of record of the flux datasets. For this reason, actual root-zone storage capacity will always exceed deficits measured through water-balance methods. Thus, in the absence of systematic error, the deficit is a lower bound on storage capacity. In addition, we make an assumption that bedrock water storage is only accessed when soil water storage is exhausted. If bedrock water is accessed at the same time as soil water storage, then our water balance calculation would result in additional underestimation of bedrock water storage capacity.

We assume that tracking the fluxes of precipitation (F_{in}) and evapotranspiration (F_{out}) into and out of a pixel, respectively, results in a lower-bound estimate of root-zone water storage deficit. In addition to the reasons listed elsewhere, this is also because the deficit is minimized by ignoring any fluxes out of the pixel that occur by mechanisms

other than evapotranspiration, such as downward drainage or runoff. We acknowledge that not all precipitation entering the root zone leaves as evapotranspiration; however, by imposing that F_{out} is represented by evapotranspiration alone, the deficit represents a lower bound on root-zone storage capacity. Including any additional fluxes in F_{out} would act to increase the deficit. As drainage is challenging to quantify, we follow deficit-based calculation methods (for example, Wang-Erlundsson et al.⁶¹) and do not attempt to quantify it. Instead, we report the lower bound of root-zone storage, which occurs when F_{out} occurs by evapotranspiration only.

Underestimating input fluxes (F_{in}) leads to overestimating S_{bedrock} and $D_{\text{bedrock},Y}$. F_{in} could be underestimated where fog, dew, irrigation or lateral flow (across pixels) is important. Fog and dew may be important sources of water, but are probably only important in a small subset of the areas where we report S_{bedrock} and $D_{\text{bedrock},Y}$. By masking locations where evapotranspiration exceeds precipitation over long time periods, we exclude locations where additional inputs to the root zone are required to explain the observed evapotranspiration data. However, lateral transport of water in the subsurface could still occur without causing evapotranspiration to exceed precipitation in the long term, in which case S_{bedrock} and $D_{\text{bedrock},Y}$ would be overestimated. By removing entire 500-m pixels where any soils exceed 1.5 m depth, we tend to exclude convergent parts of the landscape, which can have thicker soils. These areas are the most likely to experience lateral inputs of water into the root zone. Nonetheless, additional research is needed to constrain lateral water flows within hillslopes to better understand water availability to plants.

Systematic errors in the data products used in our water balance could lead to overestimation of storage. One limitation of the deficit method is that it relies on taking the integrated (summed) difference between precipitation (F_{in}) and evapotranspiration (F_{out}) such that error in either flux will accumulate and could be large relative to small deficit estimates. S_{bedrock} across the CONUS is shown in Extended Data Fig. 5. We compare this result to bedrock water storage deficit estimates obtained using the root-zone water store capacity (S_r) dataset of Wang-Erlundsson et al.⁶¹ (who used different P and ET data products at a coarser spatial resolution) shown in Extended Data Fig. 9. The patterns of bedrock water storage capacity remain similar, which suggests that the general spatial trends and magnitudes in bedrock water storage are robust to choices in input data products.

As remotely sensed ET and P datasets and in situ measurements of bedrock water storage become available, such datasets could be used to create increasingly accurate estimates of bedrock water use following the workflow presented here.

Data availability

All of the datasets generated in this study are available in the Hydroshare repository at <https://doi.org/10.4211/hs.a2f0d5fd10f14cd189a3465f72cba6f3>⁵¹. The precipitation data are available from the PRISM Climate Group⁵⁶ at <https://prism.oregonstate.edu/>. The evapotranspiration data are available from Penman–Monteith–Leuning Evapotranspiration V2 (PML_V2)⁵⁸ at https://github.com/gee-hydro/gee_PML. The snow cover data are available from NASA’s MODIS/Terra Snow Cover Daily⁶⁴ at <https://nsidc.org/data/MOD10A1/versions/6>. The soil data are available from the USDA’s gNATSGO⁴¹ database at <https://www.nrcs.usda.gov/wps/portal/nrcs/detail/soils/survey/geo/?cid=nrcseprd1464625> and in the Hydroshare repository. The landcover data are available from the USGS’s National Land Cover Database⁴⁰ at https://www.usgs.gov/centers/eros/science/national-land-cover-database?qt-science_center_objects=0#qt-science_center_objects. The biome data are available from NASA’s MODIS/Terra+Aqua Land Cover Type Yearly⁶⁵ at <https://lpdaac.usgs.gov/products/mcd12q1v006/>. The Köppen⁶⁶ climate data are available at <https://people.eng.unimelb.edu.au/mpeel/koppen.html>. The aboveground biomass¹⁹ data are available at <https://daac.ornl.gov>.

Article

gov/VEGETATION/guides/Global_Maps_C_Density_2010.html. With the exception of the gNATSGO and aboveground biomass data, all of the raster datasets are accessible via Google Earth Engine⁶². Google Earth Engine access URLs can be found in the code accompanying this study (see Code Part 2, Section 1). Source data are provided with this paper.

Code availability

Codes are available from <https://github.com/erica-mccormick/widespread-bedrock-water-use> or <https://doi.org/10.5281/zenodo.4904036>.

51. McCormick, E. L. et al. Dataset for "Evidence for widespread woody plant use of water stored in bedrock". *Hydroshare* <https://doi.org/10.4211/hs.a2f0d5fd10f14cd189a3465f72cba6f3> (2021).
52. Jackson, R. B. et al. A global analysis of root distributions for terrestrial biomes. *Oecologia* **108**, 389–411 (1996).
53. Schenk, H. J. & Jackson, R. B. The global biogeography of roots. *Ecol. Monogr.* **72**, 311–328 (2002).
54. Schenk, H. J. & Jackson, R. B. Rooting depths, lateral root spreads and below-ground/above-ground allometries of plants in water-limited ecosystems. *J. Ecol.* **90**, 480–494 (2002).
55. Fan, Y., Miguez-Macho, G., Jobbagy, E. G., Jackson, R. B. & Otero-Casal, C. Hydrologic regulation of plant rooting depth. *Proc. Natl Acad. Sci. USA* **114**, 10572–10577 (2017).
56. Daly, C. et al. Physiographically sensitive mapping of climatological temperature and precipitation across the conterminous United States. *Int. J. Climatol.* **28**, 2031–2064 (2008).
57. Daly, C., Smith, J. I. & Olson, K. V. Mapping atmospheric moisture climatologies across the conterminous United States. *PLoS ONE* **10**, e0141140 (2015).
58. Zhang, Y. et al. Coupled estimation of 500 m and 8-day resolution global evapotranspiration and gross primary production in 2002–2017. *Remote Sens. Environ.* **222**, 165–182 (2019).
59. Gan, R. et al. Use of satellite leaf area index estimating evapotranspiration and gross assimilation for Australian ecosystems. *Ecohydrology* **11**, e1974 (2018).
60. Dralle, D. N., Hahm, W. J., Chadwick, K. D., McCormick, E. L. & Rempe, D. M. Technical note: accounting for snow in the estimation of root-zone water storage capacity from precipitation and evapotranspiration fluxes. *Hydrol. Earth Syst. Sci.* **25**, 2861–2867 (2021).
61. Wang-Erlandsson, L. et al. Global root zone storage capacity from satellite-based evaporation. *Hydrol. Earth Syst. Sci.* **20**, 1459–1481 (2016).
62. Gorelick, N. et al. Google Earth Engine: planetary-scale geospatial analysis for everyone. *Remote Sens. Environ.* **202**, 18–27 (2017).
63. Singh, C., Wang-Erlandsson, L., Fetzer, I., Rockstrom, J. & van der Ent, R. Rootzone storage capacity reveals drought coping strategies along rainforest savanna transitions. *Environ. Res. Lett.* **15**, 124021 (2020).
64. Hall, D., Riggs, G. & Salomonson, V. MODIS/Terra Snow Cover Daily L3 Global 500m Grid, Version 6 [Data set] (NASA National Snow and Ice Data Center Distributed Active Archive Center, 2016).
65. Friedl, M. & Sulla-Menashe, D. MCD12Q1 MODIS/Terra+ Aqua Land Cover Type Yearly L3 Global 500m SIN Grid V006 [Data set] (NASA EOSDIS Land Processes DAAC, 2015).
66. Peel, M. C., Finlayson, B. L. & McMahon, T. A. Updated world map of the Koppen–Geiger climate classification. *Hydrol. Earth Syst. Sci. Discuss.* **4**, 439–473 (2007).
67. Harris, I., Jones, P. D., Osborn, T. J. & Lister, D. H. Updated high-resolution grids of monthly climatic observations—the CRU TS3.10 dataset. *Int. J. Climatol.* **34**, 623–642 (2014).
68. Funk, C. et al. The climate hazards infrared precipitation with stations—a new environmental record for monitoring extremes. *Sci. Data* **2**, 150066 (2015).
69. Niemeyer, R. J. et al. Spatiotemporal soil and saprolite moisture dynamics across a semi-arid woody plant gradient. *J. Hydrol.* **544**, 21–35 (2017).
70. Pedrazas, M. A. et al. The relationship between topography bedrock weathering and water storage across a sequence of ridges and valleys. *J. Geophys. Res. Earth Surf.* **126**, e2020JF005848 (2021).
71. Arkley, R. J. Soil moisture use by mixed conifer forest in a summer-dry climate. *Soil Sci. Soc. Am. J.* **45**, 423–427 (1981).
72. Zwieniecki, M. A. & Newton, M. Water-holding characteristics of metasedimentary rock in selected forest ecosystems in southwestern Oregon. *Soil Sci. Soc. Am. J.* **60**, 1578–1582 (1996).
73. Hellmers, H., Horton, J. S., Juuren, G. & O'Keefe, J. Root systems of some chaparral plants in southern California. *Ecology* **36**, 667–678 (1955).
74. Cardella Dammeyer, H., Schwinnig, S., Schwartz, B. F. & Moore, G. W. Effects of juniper removal and rainfall variation on tree transpiration in a semi-arid karst: evidence of complex water storage dynamics. *Hydrol. Process.* **30**, 4568–4581 (2016).
75. Twidwell, D. et al. Drought-induced woody plant mortality in an encroached semi-arid savanna depends on topoedaphic factors and land management. *Appl. Veg. Sci.* **17**, 42–52 (2013).
76. Davis, E. A. Root system of shrub live oak in relation to water yield by chaparral. *Proceedings of the 1977 Meetings of the Arizona Section of the American Water Resources Association and the Hydrology Section of the Arizona Academy of Sciences. Hydrol. Water Resour. Ariz. Southwest* **7**, 241–248 (1977).
77. West, A. G., Hultine, K. R., Burtsch, K. G., & Ehleringer, J. R. Seasonal variations in moisture use in a piñon-juniper woodland. *Oecologia* **153**, 787–798 (2007).
78. Seyfried, M. S. & Wilcox, B. P. Soil water storage and rooting depth: key factors controlling recharge on rangelands. *Hydrol. Process.* **20**, 3261–3275 (2006).
79. Dietrich, W. E. & Dunne, T. Sediment budget for a small catchment in mountainous terrain. *Zeitschrift Für Geomorphologie* **29**, 191–206 (1978).
80. Litvak, M. E., Schwinnig, S. & Heilman, J. L. in *Ecosystem Function in Savannas* (eds Hill, M. J. & Hanan, N. P.) 117–134 (2010).

Acknowledgements We thank R. Breunig. We acknowledge funding support from the USDA Forest Service Pacific Southwest Research Station, the National Science Foundation Graduate Research Fellowship Program and the US Department of Energy, Office of Science, Office of Biological Environmental Research under award number DESC0018039.

Author contributions E.L.M. led the data acquisition and analysis and coordinated the manuscript preparation. E.L.M. and D.M.R. drafted the initial manuscript. D.N.D., K.D.C. and W.J.H. contributed to writing and data analysis. A.K.T. contributed to data acquisition. All authors contributed to the interpretation and presentation of the results, editing and review process, and approved the final version. D.M.R. conceptualized and led the study.

Competing interests The authors declare no competing interests.

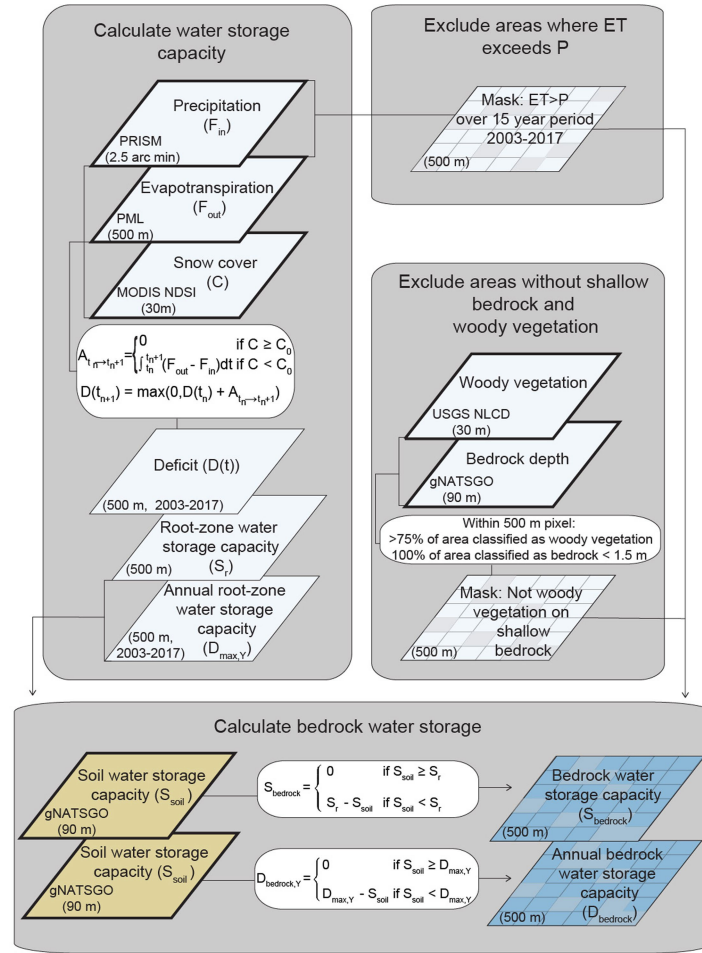
Additional information

Supplementary information The online version contains supplementary material available at <https://doi.org/10.1038/s41586-021-03761-3>.

Correspondence and requests for materials should be addressed to E.L.M.

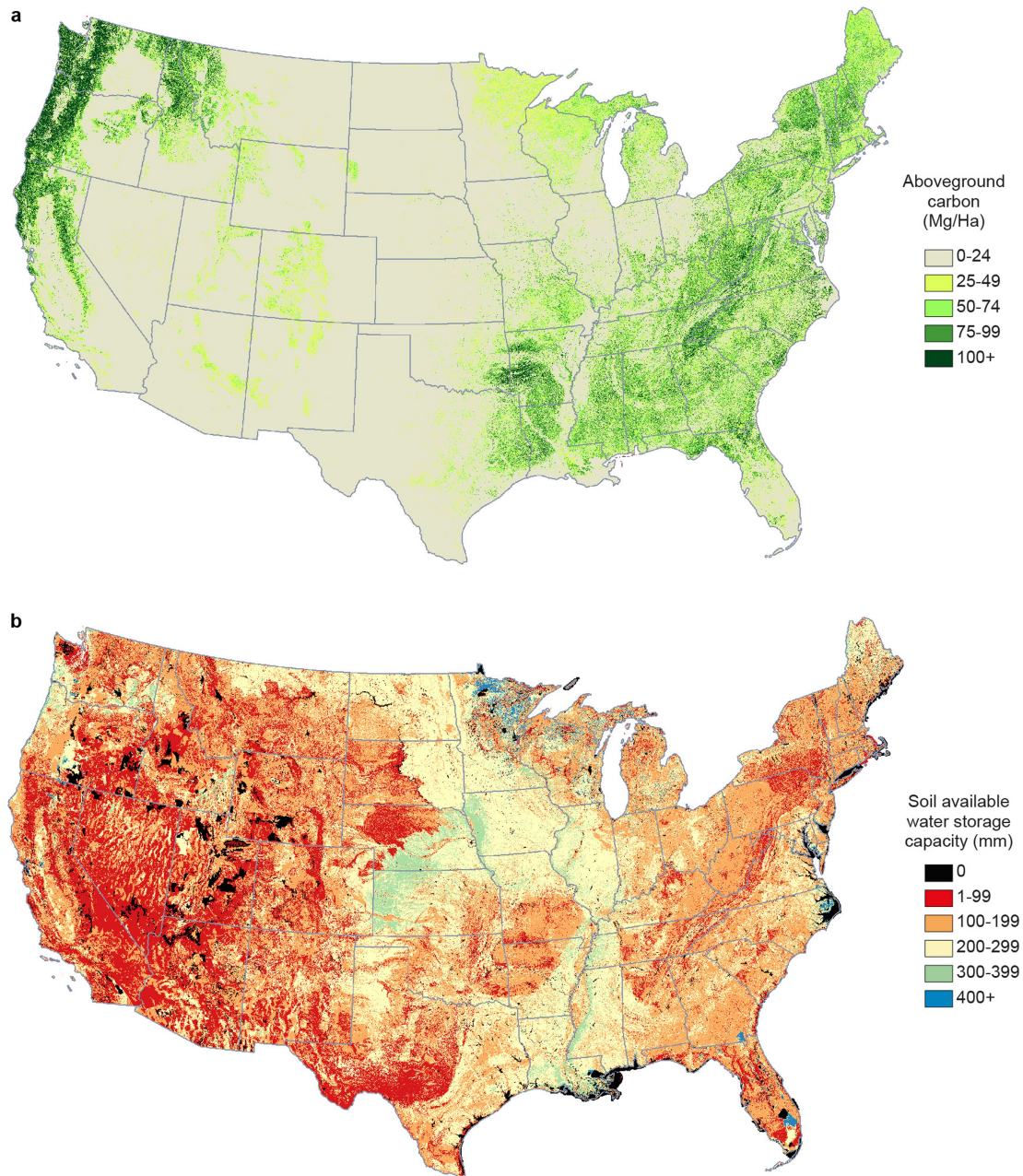
Peer review information *Nature* thanks Ying Fan, Huade Guan and the other, anonymous, reviewer(s) for their contribution to the peer review of this work. Peer reviewer reports are available.

Reprints and permissions information is available at <http://www.nature.com/reprints>.



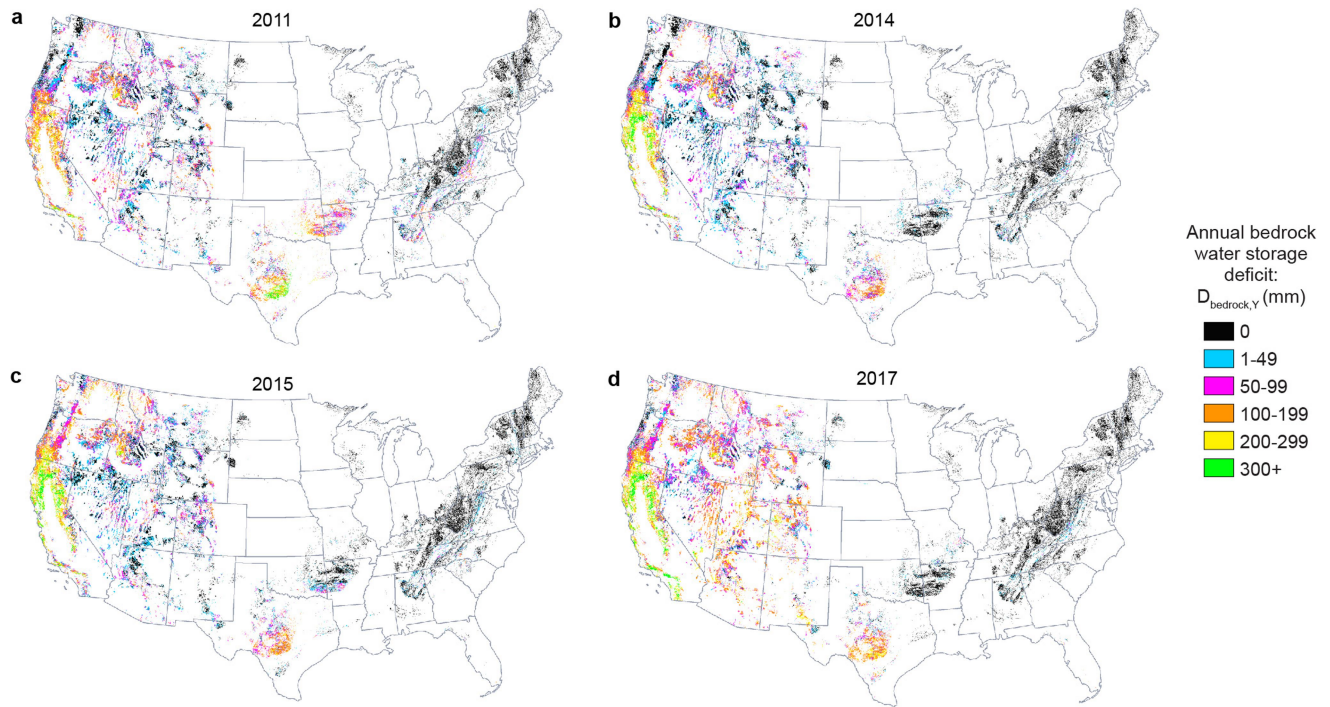
Extended Data Fig. 1 | Flow chart of the methodology for bedrock storage deficit and capacity calculations. Workflow for the calculation of total and annual bedrock water storage deficits ($S_{bedrock}$ and $D_{bedrock,Y}$, respectively). Data products (solid thick border) are reported with their spatial resolution. Calculations and thresholds are reported in white boxes (Methods). Masking

procedures exclude areas where output fluxes significantly exceed input fluxes (top right) and include areas where woody vegetation is established on shallow soils (middle right). These masks are applied to the water budget calculation (left and bottom) to arrive at conservative estimates of $S_{bedrock}$ and $D_{bedrock,Y}$ at the CONUS scale.



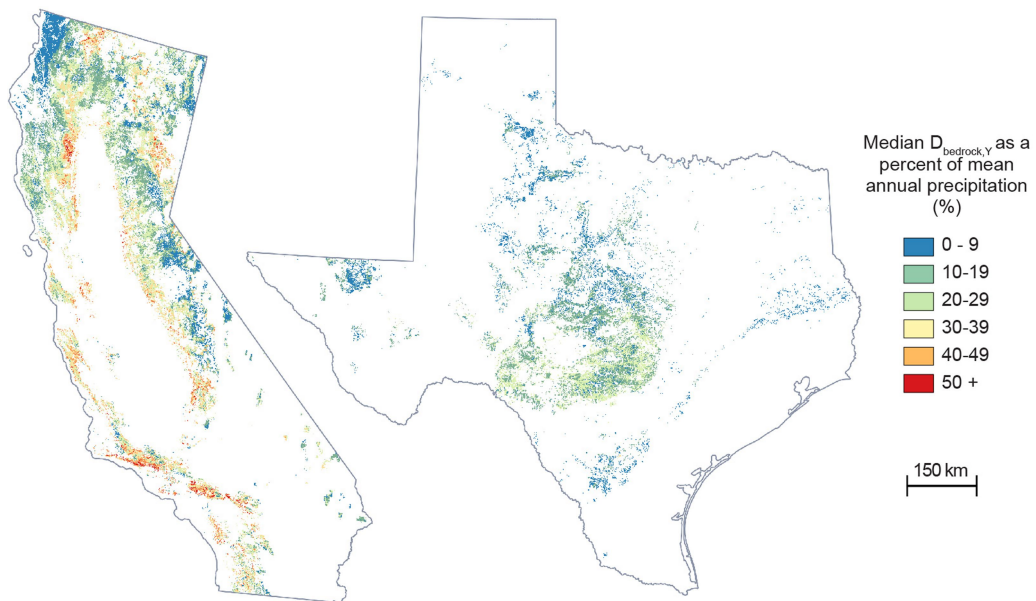
Extended Data Fig. 2 | Maps of soil and aboveground carbon input products used in this study. **a**, Aboveground carbon sourced from Spawn et al.¹⁹ (Mg ha^{-1}). **b**, Soil available water storage capacity (mm) for the CONUS. Soil

available water storage sourced at 90-m resolution from the USDA gNATSGO⁴¹ product and provided for the upper 1.5 m (Methods).



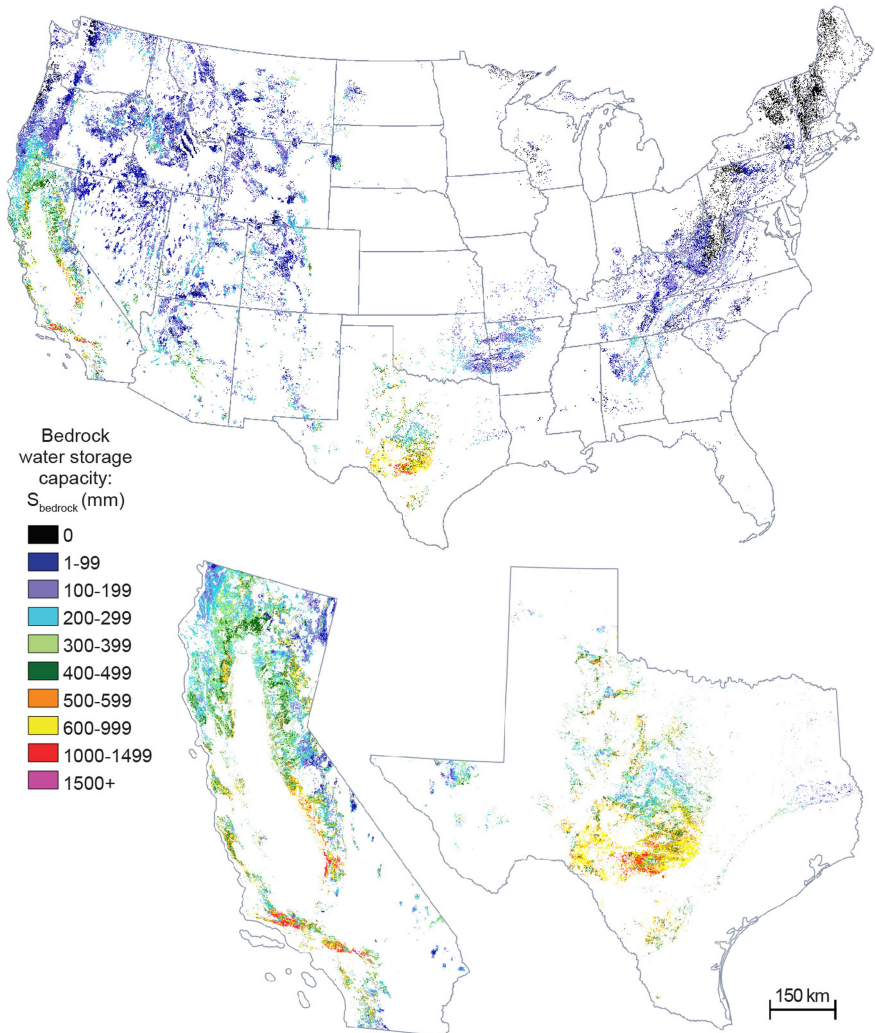
Extended Data Fig. 3 | Annual bedrock water storage deficit for four years across the CONUS. a–d, Annual bedrock water storage deficit, $D_{\text{bedrock},Y}$, for 2011 (a), 2014 (b), 2015 (c) and 2017 (d).

Article



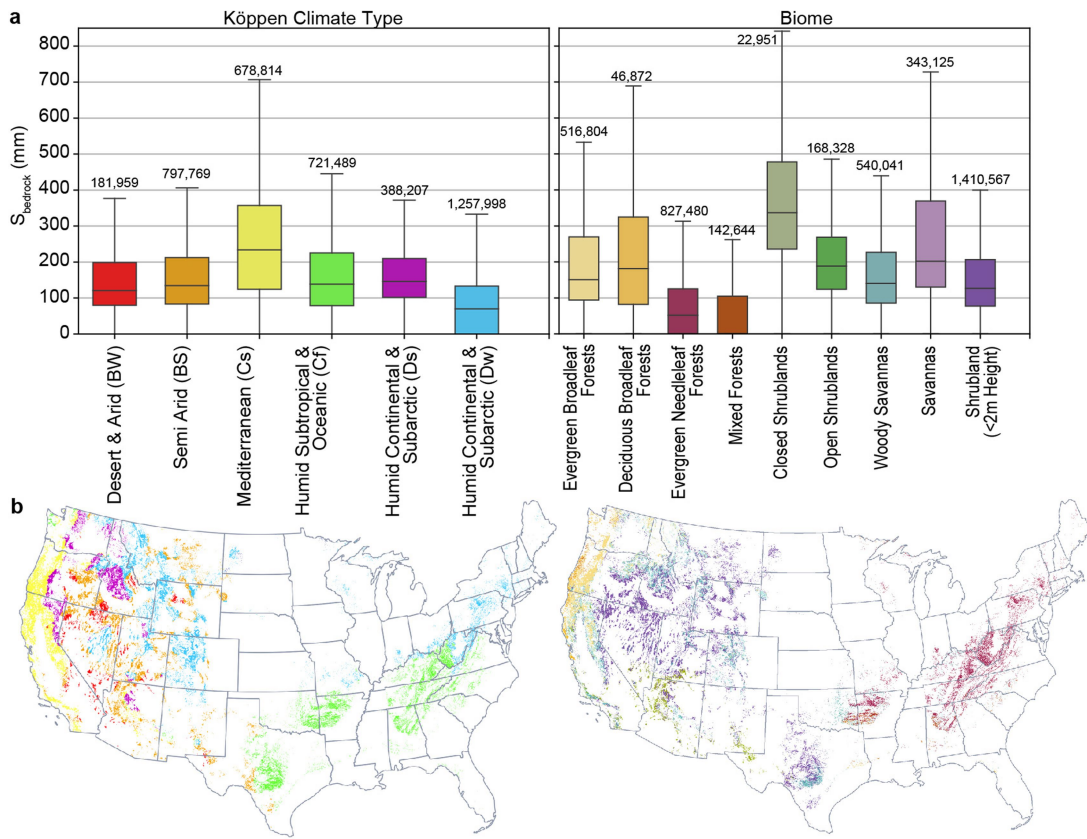
Extended Data Fig. 4 | Median annual bedrock water storage deficit constitutes more than a quarter of mean annual precipitation in some places. The magnitude of median D_{bedrock} divided by mean annual precipitation shown as a percent for California (left) and Texas (right). Mean annual

precipitation was calculated in Google Earth Engine⁶² in the Google Colaboratory environment using the PRISM Daily Spatial Climate Data set AN81d data product^{56,57}.



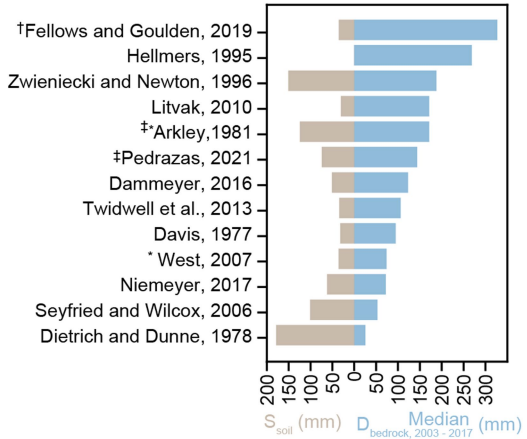
Extended Data Fig. 5 | Bedrock water storage capacity across the CONUS, California and Texas. The distribution of bedrock water storage capacity, S_{bedrock} , for locations meeting masking and calculation criteria. Where S_{bedrock} is

greater than zero, bedrock water storage is needed to explain observed ET (Methods).



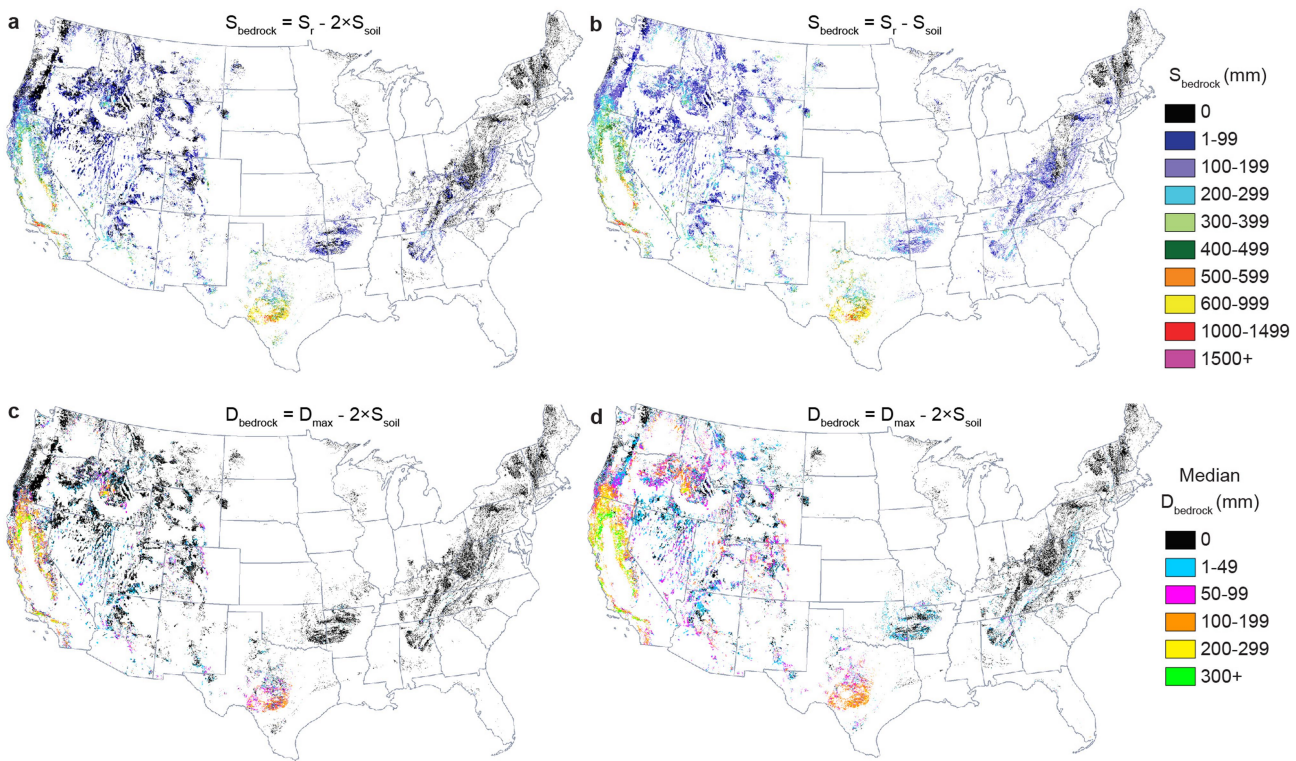
Extended Data Fig. 6 | Distribution of bedrock water storage capacity varies by Köppen climate type and biome. **a**, Boxplots show median, interquartile range and 1.5 times the interquartile range of S_{bedrock} across Köppen climate type⁶⁶ (left) and biome (MODIS landcover classifications⁶⁵) (right) for locations which meet analysis criteria (Methods). The number of pixels in each category is given above each box. The 25th percentile is non-zero for many biomes and climates. **b**, Maps indicating the locations associated with

each climate (left) and biome (right). Biome and climate subgroups with less than 2,000 km² are excluded. Summary statistics of groupings are presented in Extended Data Table 1. Post hoc tests (Kruskal–Wallis and Dunn's tests) reveal statistically significant differences ($P = <0.001$) of median S_{bedrock} between all climate group pairings and between all biome group pairings. Boxplots and statistical analyses were processed using the Google Earth Engine⁶² Python API.



Extended Data Fig. 7 | Soil and bedrock water storage capacity at locations where rock moisture use by plants has been documented. Soil water storage capacity S_{soil} (brown) and median $D_{\text{bedrock}, 2004-2017}$ (blue) for locations with documented plant use of rock moisture, that is, bedrock water storage from the unsaturated zone. Superscripts denote locations that are masked, for not being classified as woody vegetation ([#]), having soil depth greater than 1.5 m (*) or because the cumulative 2003–2017 evapotranspiration exceeds precipitation ([†]) (Methods, Extended Data Fig. 1). Data were sourced from the literature review (Methods). References for field studies: refs. ^{20,69,70,71,72,73,74,75,76,77,78,79,80}.

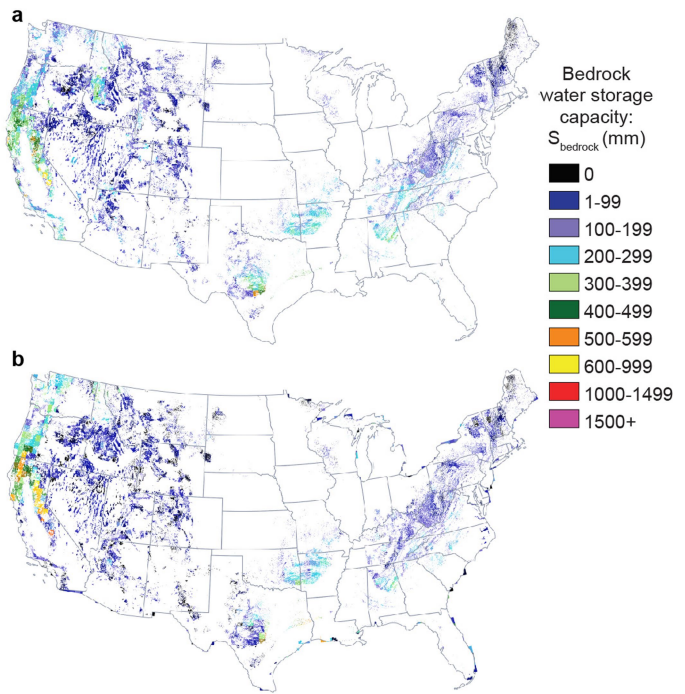
Article



Extended Data Fig. 8 | Comparison of S_{bedrock} and median D_{bedrock} to calculations using double the published soil water storage capacity values.

a, Bedrock water storage capacity (S_{bedrock}) assuming soil water storage capacity (S_{soil}) is double that reported by gNATSGO⁴¹ to account for the

possibility of soils providing water to ET at saturation, which is commonly estimated as double field capacity. **b**, S_{bedrock} without doubling of S_{soil} . **c, d**, Median annual bedrock water storage deficit, $D_{\text{bedrock}, 2003–2017}$, with doubled (c) and original (d) S_{soil} .



Extended Data Fig. 9 | Bedrock water storage capacity calculated with published values of root-zone storage capacity. **a, b,** Two versions of bedrock water storage capacity (S_{bedrock}) are calculated using root-zone storage capacity (S_r) published by Wang-Erlundsson et al.⁶¹ at a 0.5° (roughly 50 km) resolution with input and output fluxes from Climatic Research Unit Time Series version 3.22 (CRUTS3.22)⁶⁷ (**a**) and Climate Hazards Group InfraRed Precipitation with Stations (CHIRPS)⁶⁸ (**b**). To arrive at S_{bedrock} , S_{soil} is subtracted from the maximum S_r reported in Wang-Erlundsson et al.⁶¹.

Article

Extended Data Table 1 | Median bedrock water storage capacity for combinations of biomes and Köppen climate types

Köppen Climate	Biome	Median S _{bedrock}	Mean S _{bedrock}	Standard Deviation	Area km ²
Semi Arid (BSk)	Shrubland (<2m Height)	113	133	98	99253
Humid Subtropical & Oceanic (Cf)	Deciduous Broadleaf Forests	120	124	69	71399
Humid Continental (Dfb)	Deciduous Broadleaf Forests	0	18	35	59536
Humid Continental (Dfb)	Shrubland (<2m Height)	108	116	78	55507
Mediterranean (Csb)	Evergreen Needleleaf Forests	154	182	130	53710
Humid Continental (Dfb)	Woody Savannas	112	117	78	26369
Humid Continental (Dsb)	Shrubland (<2m Height)	133	149	105	24719
Arid (BWk)	Shrubland (<2m Height)	101	116	83	23595
Humid Continental & Subarctic (Df)	Deciduous Broadleaf Forests	53	70	65	23462
Humid Subtropical & Oceanic (Cf)	Shrubland (<2m Height)	410	439	199	23313
Semi Arid (BSk)	Open Shrublands	173	185	97	19065
Humid Subtropical & Oceanic (Cf)	Woody Savannas	100	132	184	18115
Humid Subtropical & Oceanic (Cf)	Savannas	509	495	342	14636
Humid Continental (Dsb)	Woody Savannas	179	197	116	13979
Humid Continental (Dsb)	Evergreen Needleleaf Forests	134	163	112	13044
Humid Continental (Dfb)	Savannas	144	153	82	12694
Humid Continental (Dfb)	Mixed Forests	0	4	21	10758
Mediterranean (Cs)	Woody Savannas	343	399	212	10204
Humid Subtropical & Oceanic (Cf)	Mixed Forests	100	100	67	10162
Mediterranean (Csb)	Woody Savannas	260	287	179	10149
Mediterranean (Cs)	Evergreen Needleleaf Forests	367	398	159	9954
Humid Continental (Dsb)	Savannas	183	212	149	9397
Semi Arid (BSk)	Woody Savannas	139	166	124	9376
Subarctic (Dfc)	Shrubland (<2m Height)	97	107	74	8898
Semi Arid (BSk)	Savannas	208	246	159	8277
Mediterranean (Csb)	Evergreen Broadleaf Forests	192	232	191	7646
Mediterranean (Cs)	Shrubland (<2m Height)	300	376	304	7431
Mediterranean (Cs)	Savannas	403	508	300	7058
Humid Continental (Dfb)	Evergreen Needleleaf Forests	107	114	64	6963
Semi Arid (BS)	Shrubland (<2m Height)	587	591	210	6670
Subarctic (Dfc)	Woody Savannas	119	132	71	5986
Mediterranean (Csb)	Shrubland (<2m Height)	182	246	225	5755
Humid Continental & Subarctic (Df)	Shrubland (<2m Height)	157	168	84	5288
Mediterranean (Csb)	Savannas	279	366	296	4929
Subarctic (Dfc)	Savannas	123	124	58	4670
Humid Continental & Subarctic (Df)	Woody Savannas	31	58	75	4402
Arid (BWk)	Open Shrublands	168	180	93	4148
Mediterranean (Csb)	Mixed Forests	112	120	106	3404
Desert & Arid (BW)	Open Shrublands	271	277	102	3202
Oceanic (Cfb)	Deciduous Broadleaf Forests	55	63	53	2978
Humid Continental & Subarctic (Ds)	Shrubland (<2m Height)	129	139	74	2931
Mediterranean (Cs)	Open Shrublands	271	284	160	2828
Oceanic (Cfb)	Evergreen Needleleaf Forests	65	72	64	2671
Semi Arid (BS)	Open Shrublands	293	338	190	2396
Semi Arid (BSk)	Evergreen Needleleaf Forests	169	225	220	2200

Median S_{bedrock} and standard deviation for combinations of biomes and Köppen climate types ranked from high to low median S_{bedrock}. The area represented by each biome and climate is reported. Areas less than 2,000 km² are excluded. Bedrock water storage may be particularly important in semiarid shrublands, Mediterranean savannahs and Mediterranean needleleaf forests.